Research Article

Ahmed Alhumaidan, Hamsakutty Vettikalladi*, Meshal Bahammam, Tariq Alrashied and Majeed Alkanhal

Design of a vertically stacked double Luneburg lens-based beam-scanning antenna at 60 GHz

https://doi.org/10.1515/eng-2024-0103 received April 18, 2024; accepted November 25, 2024

Abstract: This article presents the design of a 60 GHz beam-scanning antenna system with a coverage range of 50–100 m for high-speed indoor communication systems. The design incorporates beam-scanning techniques to meet the coverage requirements while minimizing system cost and size. The system comprises a substrate-integrated waveguide for stable operation, a printed log periodic dipole array operating at 60 GHz with a 10 GHz bandwidth (54–67 GHz), which provides a 6.99 dB directivity. Adding a vertically stacked double Luneburg lens improves pattern coverage performance and increases the system directivity to 17 dBi (14.8 dB gain) with a 4.6° beam width. With 37 source antennas, it can provide a total beam coverage area of 170°, which is highly suitable for future high-speed indoor communication.

Keywords: luneburg lens antenna, 60 GHz, beam scanning, high-gain antenna, SIW

1 Introduction

Fifth-generation technologies are being researched to meet consumer, service, and corporate expectations. The essential goal of 5G technology is to provide higher coverage with minimal power usage and cheap cost by using a high-frequency band along with a large bandwidth for enhancing data transfer rates. To address the lack of available bandwidth, higher operating frequencies in the millimeter wave (mm-Wave) region of the electromagnetic spectrum are being considered. However, the short-range

increasing the infrastructure cost due to the need for more cells to cover a specific location [1,2]. Beam-scanning techniques, such as phase variation, offer a solution to increase wide-angle coverage. In a previous study [3], a beam-scanning lens antenna is proposed, but the beamscanning range is only ±60°, and also the gain tolerance is as high as 3.6 dB. Also, in the literature [4,5], a superstrate/metasurface antenna is proposed for high gain, but this cannot be used for beam tilting or scanning. Hybrid designs, including lens antennas, are of interest due to their high gain, low cost, low profile, and ease of integration. One such low-cost and high-gain antenna manufacturing technique is elaborated by Bor et al. [6]. Another passive beam steering millimeter wave antenna is detailed by Das et al. [7], but the maximum steering angle is ±30° only. Here, passive beam-steering is achieved with the change in orientation of the metasurface, which reverses the sequence of unit cells that avoids the need for active components, which leads to a bulky structure.

coverage of higher frequency bands poses a challenge,

This work aims to design a wide-band, high-gain antenna system using a Luneburg lens integrated with a log-periodic dipole array (LPDA) and a substrate-integrated waveguide (SIW). The goal is to achieve a system gain higher than 14 dB (directivity higher than 16 dB) with wide beam scanning of around 170°, while considering the total cost and compact size of the system. The design process involves stages, including SIW design, LPDA design used for increasing the bandwidth, and Luneburg lens design for increasing the directivity and beam scanning. The theoretical design optimization of a multi-shell luneburg lens is well illustrated in a study by Fuchs et al. [8]. The design and practical verification of a three-dimensional printed flat Luneburg lens is demonstrated by Che et al. [9] with high gain but a limited beam-scanning capacity of ±30°. There are several source antenna types suitable for this work, including the Yagi-Uda, Microstrip Patch, and LPDA. While the Yagi-Uda antenna offers high gain and narrow beamwidth, its limited bandwidth may not be ideal. The microstrip patch antenna is compact and lightweight but has limited bandwidth. The LPDA provides a wide bandwidth and high directivity and

Ahmed Alhumaidan, Meshal Bahammam, Tariq Alrashied, Majeed Alkanhal: Electrical Engineering Department, College of Engineering, King Saud University, Riyadh, Saudi Arabia

^{*} Corresponding author: Hamsakutty Vettikalladi, Electrical Engineering Department, College of Engineering, King Saud University, Riyadh, Saudi Arabia, e-mail: hvettikalladi@ksu.edu.sa

is cost-effective in fabrication [10]. The chosen approach for beam-scanning design is the dielectric focusing architecture, utilizing a dielectric lens. This architecture offers beam switching and scanning capabilities, enhances antenna gain and performance, and provides cost-effective material and manufacturing options. The design comprises three major parts: SIW to avoid feed radiation, LPDA, and flat Luneburg lens. SIW improves overall performance and stability, as described in the research studies [11,12], LPDA offers the desired operating bandwidth and directive source radiation beam, and the flat Luneburg lens enhances antenna directivity, in addition to beam scanning and shaping capabilities. Section 2 provides the methodology used for the design, and Section 3 details the simulation of the proposed antenna system and its results. The prototyping of the antenna is provided in Section 4 with a comparison of previous works. Finally, Section 5 provides the conclusion remarks.

2 Methodology

2.1 SIW design

SIW is a low-cost and highly efficient integrated planar architecture that overcomes the limitations of traditional waveguide technology. SIW is designed by incorporating metallic through holes or slot trenches on a flat substrate, as seen in Figure 1, providing advantages such as cost-effectiveness, compact size, light-weight, and ease of manufacturing. To design the SIW, the dimensions and parameters of the rectangular waveguide are determined based on the TE10 mode and the cutoff frequency. Integration and interconnect techniques of planar and non-planar structures are demonstrated by Wu [13]. In previous studies [14–16], the design and propagation characteristic of SIW are detailed.

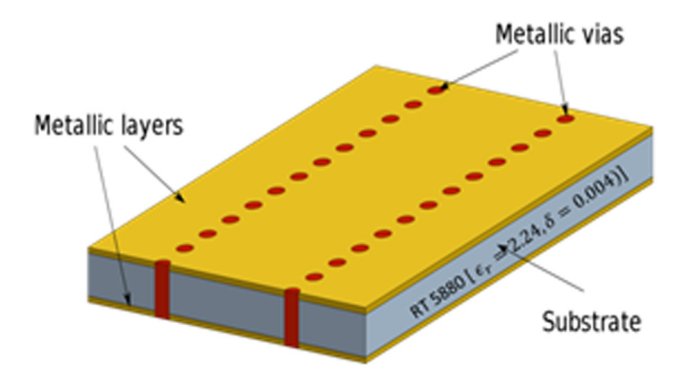


Figure 1: SIW structure.

2.2 Source antenna design

The LPDA antenna is chosen for its wide bandwidth, high gain, efficiency, and ease of integration. The LPDA design involves determining the scale factor, spacing factor, and the number of dipole elements. The design parameters such as the lengths, widths, and spacing between the dipole components are calculated based on the desired bandwidth and directivity. The LPDA design is optimized to achieve the desired performance metrics. The detailed analysis of LPDA design is well illustrated in previous studies [17,18]. The integration of the LPDA and SIW antennas was accomplished through a tapered connection, ensuring seamless transition and proper feeding. Transition from microstrip to waveguide is demonstrated in the literature [19,20].

2.3 Luneburg lens design

A Luneburg lens is introduced to enhance antenna gain and provide beam scanning and shaping capabilities, while reducing the overall size of the antenna. The lens design consists of different layers with specific dielectric constants and radius, as illustrated in Figure 2. The radius and permittivity of each layer are determined using mathematical equations based on the number of layers. The Luneburg lens is designed to focus the radiation pattern in the H-plane and is fabricated using a novel, low-cost, and easy technological approach. The lens is evaluated in the 60 GHz bandwidth spectrum, and its behavior is analyzed using Airex PXc 245 foam materials.

The different layer radii of the Luneburg (r_i) lens and the different dielectric permittivities (ε_i) of each layer can be obtained from the equations below, where N is the number of layers [8]:

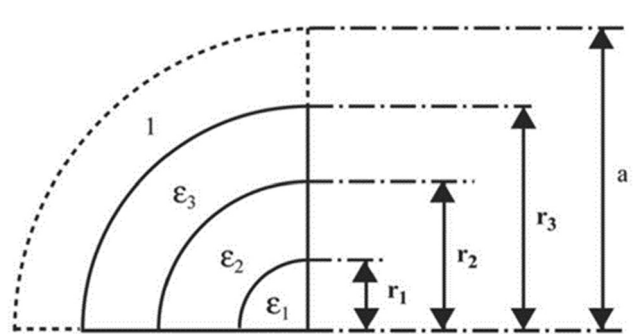


Figure 2: Cross-sectional view of Luneburg lens.

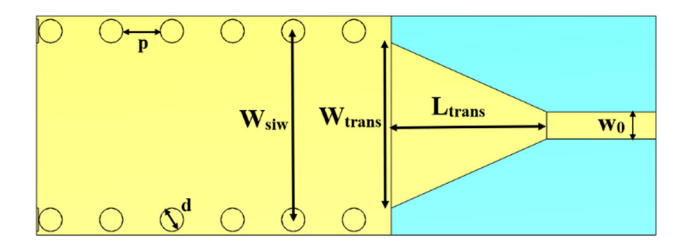


Figure 3: SIW structure with transition and feed.

$$\varepsilon_i = 2 - (2i - 1)M,$$

$$r_i = \sqrt{2 - \varepsilon_i + M},$$

$$M = \frac{1}{2N + 1}.$$

3 Simulation

3.1 SIW simulation

The simulation was carried out in CST Microwave Studio with a lambda/20 mesh size. The SIW simulation involves designing and optimizing a 60 GHz SIW using Roger RT/Duroid5880 as the substrate material ($\varepsilon_r = 2.23$, $\delta = 0.003$, h = 0.127 mm) with copper thickness $M_{\rm t} = 0.018$ mm. The SIW transmission line, modeled using CST Microwave Studio, is shown in Figure 3 with its optimized parameter tabulated in Table 1. Figure 4 shows excellent performance with a cutoff frequency of 44 GHz.

The analysis of scattering parameters (S_{11} , S_{21}) demonstrates a strong match between the SIW and antenna design at 60 GHz (above 48 GHz).

3.2 LPDA simulation

In the LPDA simulation, a log periodic antenna (LPDA) design is presented. The optimized LPDA design incorporates changes in the leg values (a_n, b_n) and leg spacing. The LPDA structure which shown in Figure 5 is designed to optimise the performance with a wide bandwith and directivity, and its dimensions are provided in Table 2, is based on a Roger RT/Duroid 5,880 substrate with dielectric

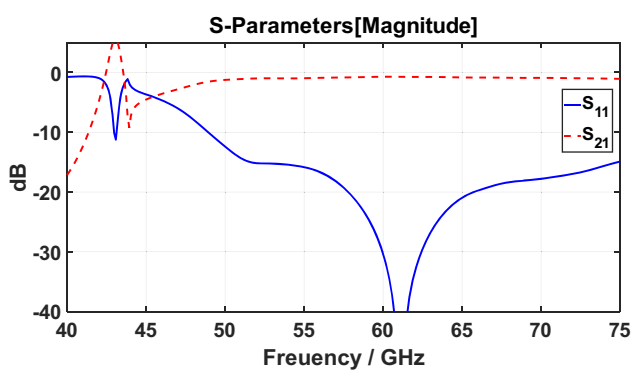


Figure 4: SIW return loss plot vs frequency.

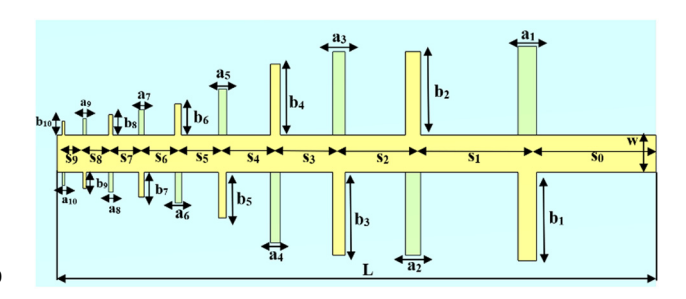


Figure 5: LPDA structure with dimensions.

Table 2: LPDA dimensions

Parameters		<i>a_n</i> (mm)	<i>b_n</i> (mm)	<i>S_{n-1}</i> (mm)
n	1	0.17	0.82	1.20
	2	0.14	0.77	1.07
	3	0.11	0.77	0.69
	4	0.09	0.66	0.59
	5	0.07	0.42	0.49
	6	0.06	0.29	0.41
	7	0.05	0.23	0.34
	8	0.04	0.19	0.29
	9	0.03	0.15	0.24
	10	0.03	0.12	0.20
L (mm)			5.58	
W (mm)			0.34	

parameters (ε_r = 2.23, δ = 0.003) with a thickness of (h = 0.127 mm), which helps in reducing surface waves.

Table 1: SIW parameters dimension

Parameters	W _{siw} (mm)	W _{trans} (mm)	W ₀ (mm)	L _{trans} (mm)	<i>P</i> (mm)	D (mm)
Dimensions (mm)	2.41	2.11	0.34	2	0.48	0.3

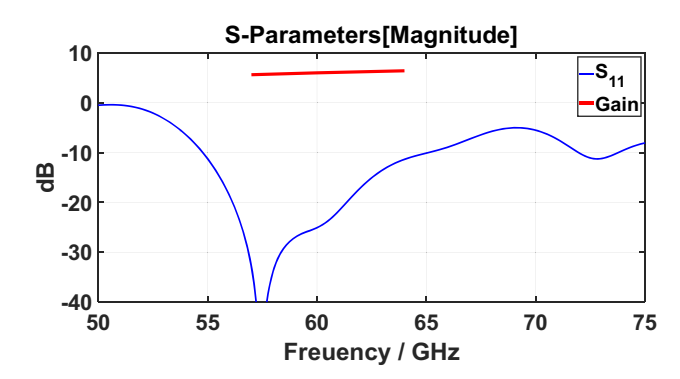


Figure 6: LPDA gain and S₁₁ vs frequency plot.

The optimized LPDA design achieves a bandwidth of 9 GHz below –10 dB. The optimized S-parameter is plotted along with the antenna gain in Figure 6, highlighting the performance characteristics.

3.3 LPDA, SIW, and Luneburg lens (system) simulation

This section focuses on the integration of the optimized LPDA and SIW components with the Luneburg lens to form a complete system. A tapered transition is introduced between the SIW and LPDA antenna to ensure a smooth connection, as shown in Figure 7. The thickness of metal on either side of the substrate is 0.127 mm. The optimized dimensions are displayed in Table 3.

The optimized structure achieves a wide bandwidth of 20 GHz at 60 GHz, as depicted in Figure 8. Additionally, a directivity of 6.99 dB and a half-power beamwidth (HPBW) of 59° are achieved.

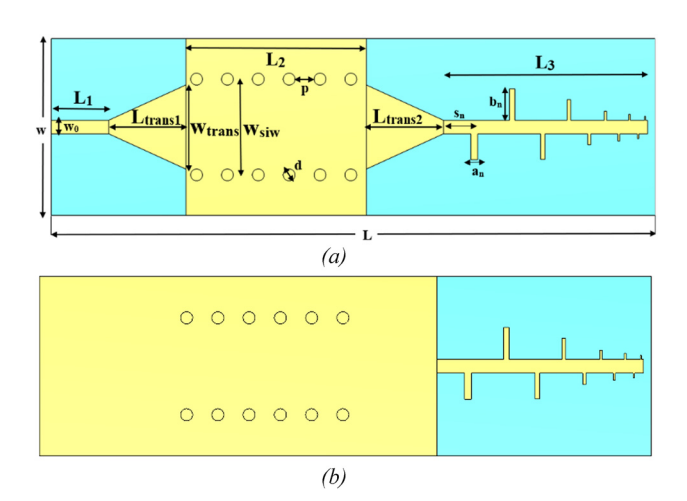


Figure 7: Single SIW antenna with LPDA: (a) top view and (b) bottom view.

Table 3: Single antenna element dimensions

Parameters		<i>an</i> (mm)	<i>bn</i> (mm)	<i>Sn-</i> 1 (z mm)	<i>Ln</i> (mm)	Ltrans, n (mm)
n	1	0.17	0.65	0.78	1.4	2
	2	0.14	0.79	0.96	4.56	1.95
	3	0.11	0.64	0.78	5.16	
	4	0.09	0.52	0.66		
	5	0.07	0.28	0.51		
	6	0.06	0.23	0.41		
	7	0.05	0.18	0.33		
	8	0.04	0.15	0.27		
	9	0.03	0.12	0.22		
	10	0.03	0.10	0.18		
L (mm)	15.27					
W (mm)	4.46					

3.4 Luneburg lens and full system simulation

Next, the simulation focuses on the Luneburg lens and the performance of the full system comprising multiple antennas. The lens design process involves optimizing the number of layers and choosing the optimal structure based on the radiation pattern, which can be seen in Figure 9 with one source element. The optimized dimensions of the lens are tabulated in Table 4. The results indicate that a six-layer lens provides a smoother radiation pattern.

The optimized single antenna element with a lens is achieved with specific parameters, resulting in a directivity of 16.5 dB and a HPBW of 4.6°, as illustrated in Figure 10 at 60 GHz. Additionally, Figure 11 shows a gain of 14.5 dB, which complements the performance characteristics of the antenna element.

The phase distribution of a Luneburg lens is a key characteristic that contributes to its unique focusing properties. In a Luneburg lens, the refractive index varies

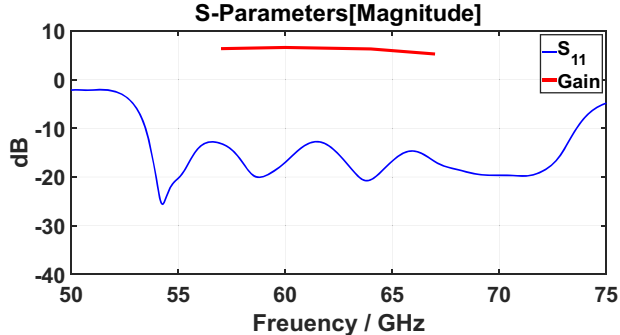


Figure 8: Antenna gain and S₁₁ vs frequency plot.

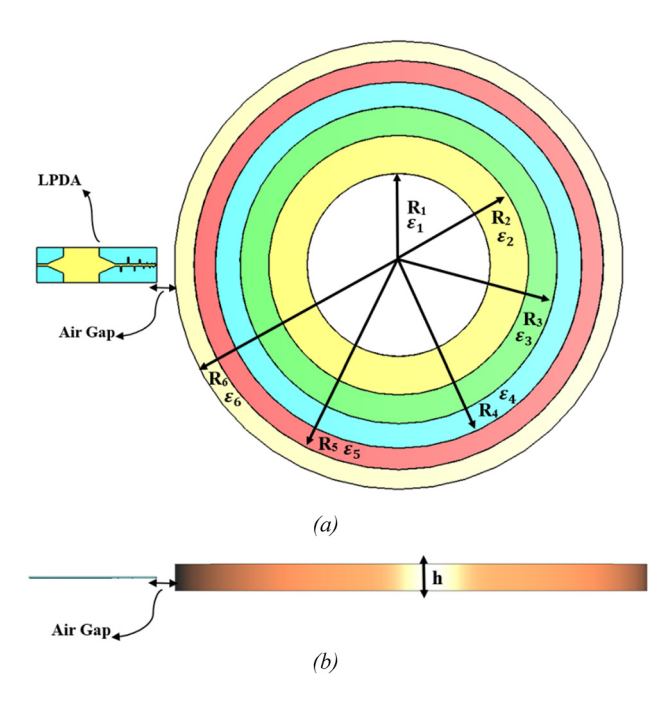


Figure 9: Luneburg lens structure with a single feed: (a) top view and (b) side view.

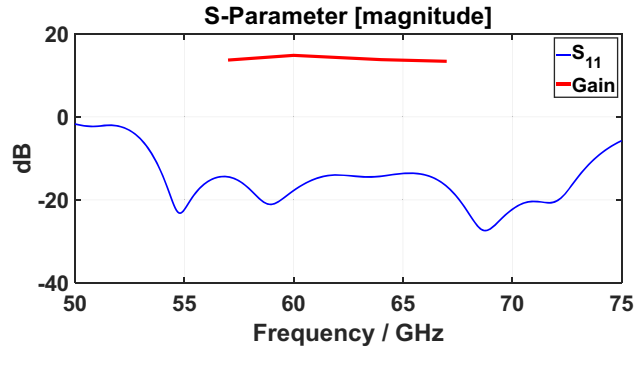


Figure 11: Gain and S11 vs frequency plot.

radially from the center to the outer surface, creating a gradient lens. The phase distribution across the lens is such that it compensates for the spherical aberration that would occur in a simple lens with a uniform refractive index.

For a Luneburg lens, the phase distribution is typically designed to be radially symmetric. The phase distribution is such that the wavefronts passing through different

Table 4: Luneburg lens parameters

Parameters	Rad	ius (mm)	Permittivity (ϵ)	Loss tangent
Layer number	1	11.625	1.92	0.015
	2	16.5	1.77	0.014
	3	20.15	1.62	0.013
	4	23.275	1.46	0.01
	5	26	1.31	0.008
	6	28.5	1.15	0.007
Lens thickness (h) (mm)			3.2	
Air gap (mm)			2.6	

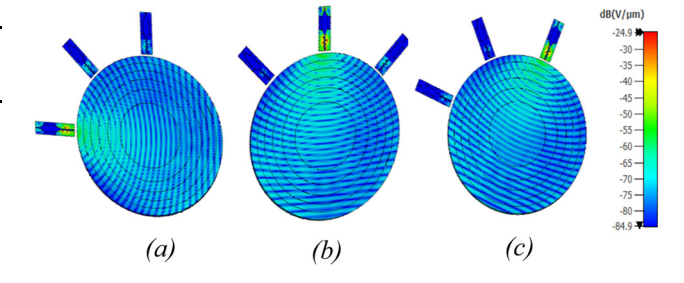


Figure 12: Phase distribution. (a) 90°, (b) 0°, (c) 45°.

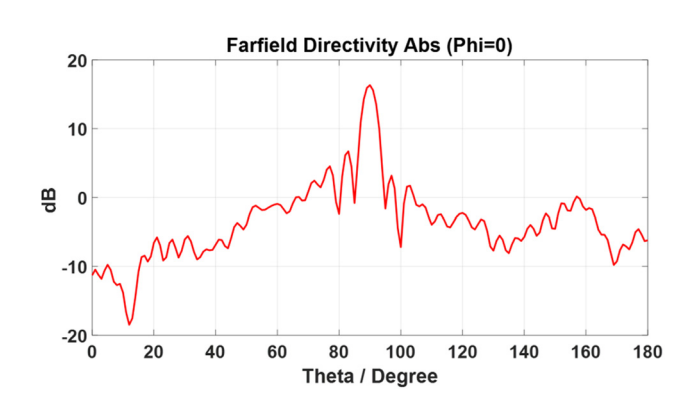


Figure 10: Far-field directivity plot.

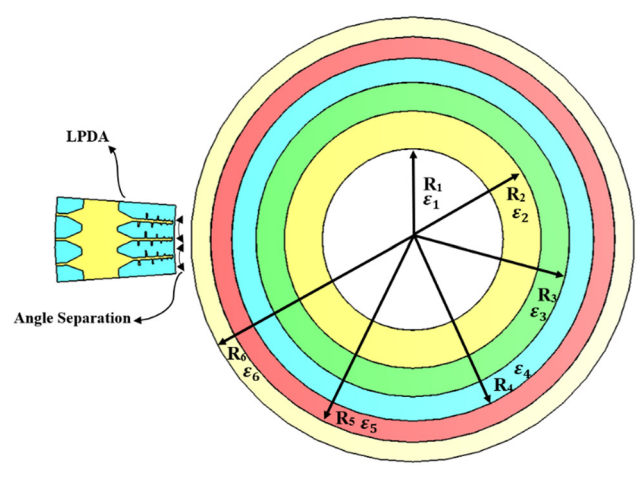


Figure 13: Adjacent antenna structure.

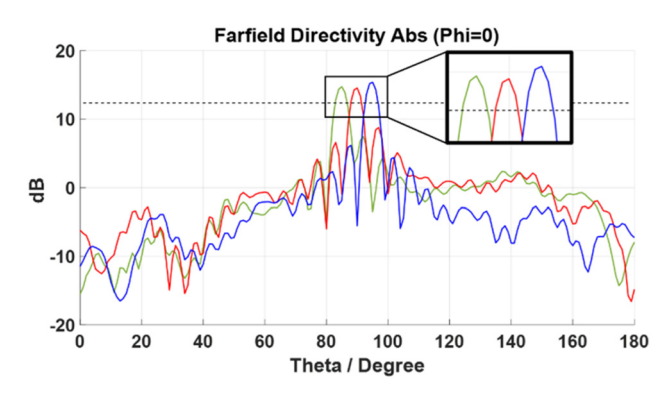


Figure 14: Far-field plot without coverage.

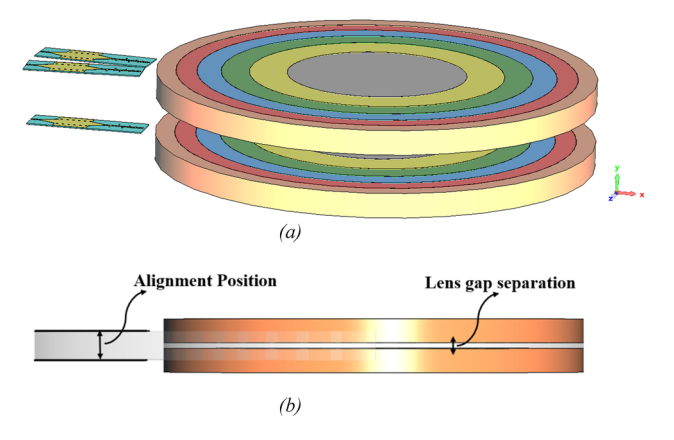


Figure 15: Doubled stacked Luneburg lens: (a) top view and (b) side view.

regions of the lens converge at the same focal point, resulting in the effective focusing of incoming waves.

The phase distribution of the Luneburg lens with different feeding angles (90°, 0°, and 45°) is shown in Figure 12.

Expanding the system to three antenna elements, as shown in Figure 13, their behavior in the far field is examined for multiple-angle separations. The adjacent placement of the three antennas was tested with varying separation

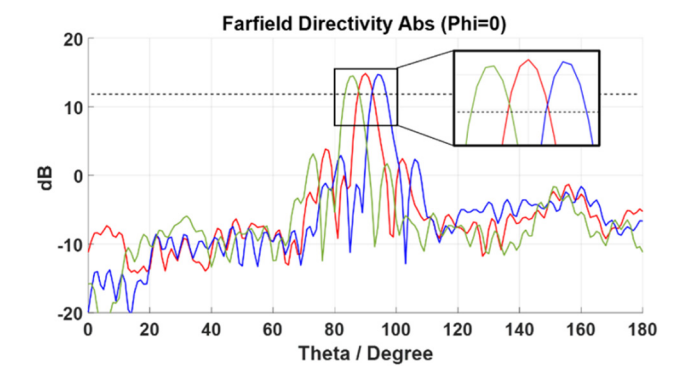


Figure 16: Far-field plot with coverage.

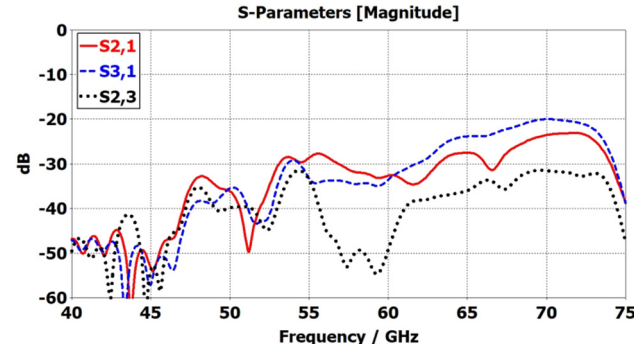


Figure 17: S-parameter of three-adjacent antenna elements to show coupling effect.

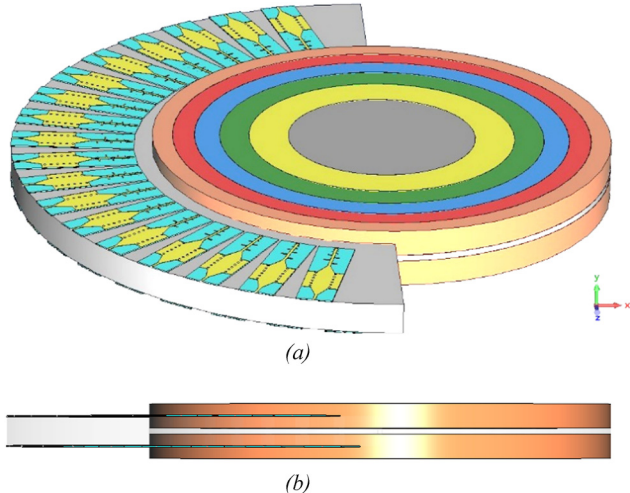


Figure 18: Full system doubled stacked Luneburg lens with supporting foam with complete feed: (a) top view and (b) side view.

angles to achieve $3\,\mathrm{dB}$ overlapping. However, the results provided in Figure 14 show a version of the incomplete coverage and increased side lobe levels when setting the separation angle to be 4.5° .

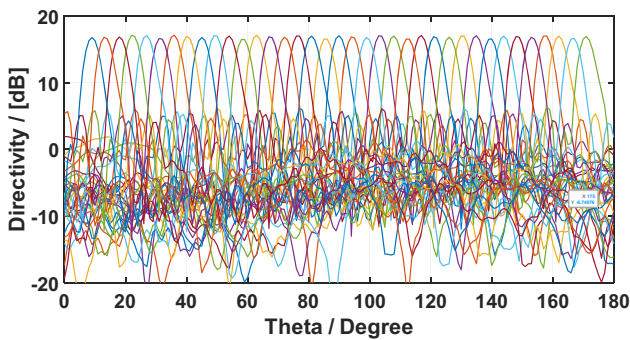


Figure 19: Full system far-field directivity plot.

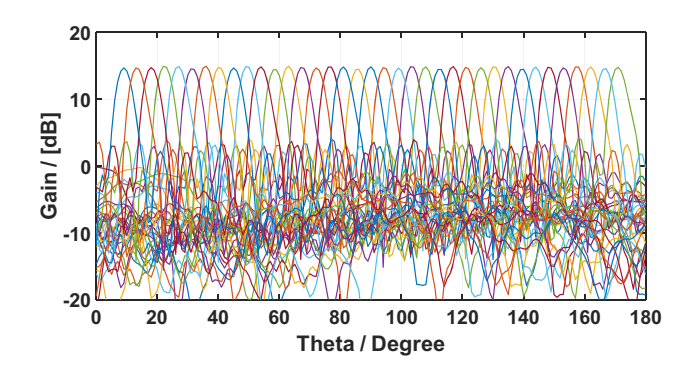


Figure 20: Full system far field gain plot.

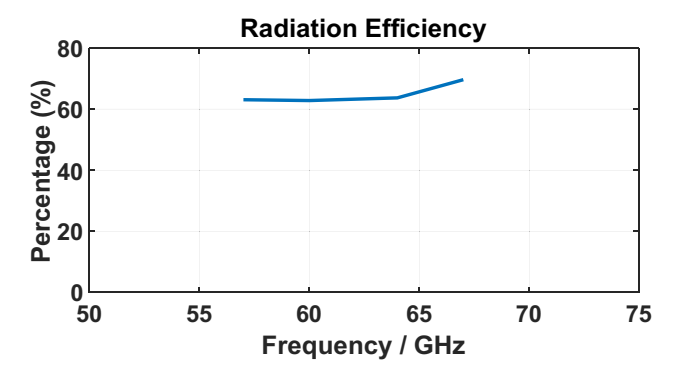


Figure 21: Efficiency vs frequency plot.

To address this issue of incomplete coverage, we first propose a new idea of a vertically stacked double Luneburg lens with feed elements in the lower and upper lens concept is introduced as shown in Figure 15 with an angle separation of 9° between two feed elements in the same lens and the angle between the adjacent feed element in the lower and upper lens is 4.5°.

The optimization process focuses on determining the vertical alignment and separation distance between the

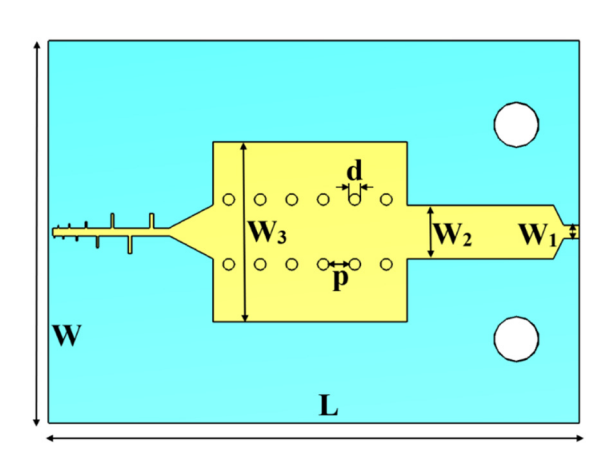


Figure 22: Simulation structure.



Figure 23: Prototype.

Table 5: Prototype feed dimensions

Parameter		(mm)
W_n	1	0.60
	2	2.38
	3	8.00
D		0.50
P		0.90
L		23.59
W		17.00

lenses. The best results are obtained when the antennas are aligned in the middle, and the optimized vertical lens separation is 0.75 mm. The directivity and gain for different frequencies are analyzed, and the one-dimensional far-field pattern is observed at 60 GHz, which can be seen in Figure 16.

Additionally, the coupling between the three adjacent antenna elements was minimal and reached a value of -20 dB on the operating frequency, as shown in Figure 17.

Finally, the full system integration consists of 37 antenna feeds in both lenses, providing a coverage area of 170°, as

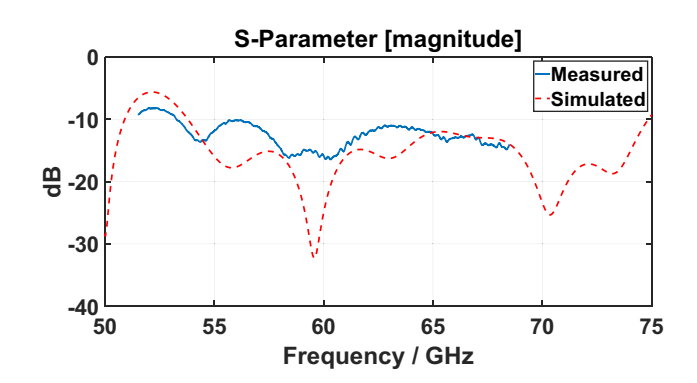


Figure 24: Return loss vs frequency plot of the prototype.

8 — Ahmed Alhumaidan *et al.* DE GRUYTER

Table 6: Comparative analysis between the proposed antenna and state-of-the-art antenn

Ref.	Frequency <i>f</i> (GHz)	Bandwidth (BW)	Gain (dB)	Scanning range	Efficiency η (%)
[21]	60	58/67	11.7	21° (38° to 7°)	90
[22]	60	50/75	14.2	49° (-9° to 40°)	75
[23]	60	52/63	11.4	9° (12° to 3°)	_
[24]	60	55/65	14.5	120° (-72° to 48°)	88.2
Proposed	60	54/67	14.8	170° (-85° to 85°)	63

shown in Figure 18. The structure of both lenses and feeds is supported using FR-3703 polyurethane foam (ε_r = 1.04, tans δ = 0.00170), as seen in the same figure. The performance is evaluated in terms of directivity, gain, and overlapping. The results demonstrate a difference of \geq 13 dB between the main and side lobes, achieving 3 dB overlapping as illustrated in Figures 19 and 20, with a directivity of 17 and 14.8 dB gain, respectively.

The optimized system showed consistent performance throughout the operating frequency range with an efficiency reaching 63%, as shown in Figure 21.

4 Prototyping

The fabricated design of the antenna yielded promising results. Figure 22 displays the simulated structure. Due to the limitations in manufacturing capabilities in our lab, the substrate thickness was increased to 0.79 mm (h = 0.79 mm). Consequently, the feed is optimized to match the new thickness, with the optimized dimensions provided in Table 5.

The prototype is depicted in Figure 23 with SIW and LPDA. The LPDA antenna is printed using LPKF laser and electronics PhotoMat S-103, and the S-parameter is measured using a Keysight vector network analyzer (PNAX; N5247A). The measured return loss closely matched the simulated results (55–75 GHz), as shown in Figure 24, validating the accuracy of the design and manufacturing procedures.

These findings provide strong evidence for the practical applicability of the fabricated design in this microcell technology, highlighting the effectiveness of the beamscanning antenna in enabling precise and efficient control of electromagnetic radiation. This research contributes to the advancement of high-speed antenna networks, facilitating the development of reliable and high-performance 5G microcell technology.

A comparison of the proposed antenna with other work is given Table 6, which clearly shows that the proposed antenna achieved better performance in terms of a gain of 14.8 dB and a pattern coverage of around 170° compared with state-of-the-art antenna designs. The other works in the literature show a maximum beam scanning angle of only 120°. Also, the gain is maximum in this work. This antenna is cost-effective and easy to fabricate compared to others mentioned in the table. Due to this wide-angle scanning capability, this work is suitable for high-speed wireless communication applications.

5 Conclusion

This study presents the design and simulation of a beam-scanning antenna for future high-speed short-range communication systems operating at 60 GHz. The system incorporates an SIW, an LPDA antenna, and a Luneburg lens. The optimized SIW and LPDA antenna achieve directivities of 5.95 and 6.99 dB at 60 GHz, respectively, with improved bandwidth and radiation patterns. The addition of a vertically stacked double Luneburg lens enhances the system's directivity to 17 dB. Simulation results demonstrate wide-angle beam scanning and good radiation efficiency, making the antenna suitable for power-efficient future high-speed applications. The integrated system comprises 37 antenna elements achieving around 170° coverage with beam-scanning capability. Hence, it offers a promising candidate for real-world implementation in high-frequency 60 GHz communication systems.

Acknowledgements: This work was supported by the National Plan for Science, Technology and Innovation (MAA-RIFAH) and King Abdulaziz City for Science and Technology, Saudi Arabia, under Award 13-ELE1184-02-R. The authors are grateful for the reviewer's valuable comments that improved the manuscript.

Funding information: This work was supported by the National Plan for Science, Technology and Innovation (MAA-RIFAH) and King Abdulaziz City for Science and Technology, Saudi Arabia, under Award 13-ELE1184-02-R.

Author contributions: All authors have accepted responsibility for the entire content of this manuscript and consented to its submission to the journal, reviewed all the results, and approved the final version of the manuscript. Ahmed Alhumaidan, Meshal Bahammam, and Tariq Alrashied did all the simulation and manufacturing of the work. Hamsakutty Vettikalladi and Majeed Alkanhal did the overall supervision of the work and manuscript preparation.

Conflict of interest: Authors state no conflict of interest.

Data availability statement: All data generated or analyzed during this study are included in this published article.

References

- Lawrence NP, Ng BW, Hansen HJ, Abbott D. 5G terrestrial networks: Mobility and coverage – Solution in three dimensions. IEEE Access. 2017;5:8064–93. doi: 10.1109/ACCESS.2017.2693375.
- [2] Rangan S, Rappaport TS, Erkip E. Millimeter-wave cellular wireless networks: Potentials and challenges. Proc IEEE. 2014;102(3):366–85. doi: 10.1109/JPROC.2014.2299397.
- [3] Wang HF, Wang ZB, Wu ZH, Zhang YR. Beam-scanning lens antenna based on elliptical paraboloid phase distribution metasurfaces. IEEE Antennas Wirel Propag Lett. 2019;18(8):1562–6. doi: 10.1109/ LAWP.2019.2922695.
- [4] Vettikalladi H, Lafond O, Himdi M. High-efficient and high-gain superstrate antenna for 60-GHz indoor communication. IEEE Antennas Wirel Propag Lett. 2009;8:1422–5. doi: 10.1109/LAWP. 2010.2040570.
- [5] Das P, Singh AK. Gain enhancement of millimeter wave antenna by ultra-thin radial phase gradient metasurface for 5G applications. IETE J Res. 2023;69:2400–8. doi: 10.1080/03772063.2023.2191998.
- [6] Bor J, Lafond O, Merlet H, Le Bars P, Himdi M. Foam based Luneburg lens antenna at 60 GHz. Prog Electromagn Res Lett. 2014;44:1–7. doi: 10.2528/PIERL13092405.
- [7] Das P, Singh AK, Mandal K. Beam-steering of millimeter wave antenna using linear phase gradient metalens for 5G applications. Int J RF Microw Comput Eng. 2022;32(12):e23459. doi: 10.1002/ mmce.23459.
- [8] Fuchs B, Le Coq L, Lafond O, Rondineau S, Himdi M. Design optimization of multishell Luneburg lenses. IEEE Trans Antennas Propag. 2007;55(2):283–9. doi: 10.1109/TAP.2006.889849.
- [9] Che X, Gao J, Li Z. 3-D printed high-gain elliptic flat Luneburg lens. Results Phys. 2024;57:1–9. doi: 10.1016/j.rinp.2024.107350.

- [10] Balanis CA. Antenna theory: analysis and design. 3rd edn. NJ: John Wiley; 2005.
- [11] Wu K, Deslandes D, Cassivi Y. The substrate integrated circuits a new concept for high-frequency electronics and optoelectronics. 6th International Conference on Telecommunications in Modern Satellite, Cable and Broadcasting Service. Telsiks; 2003. p. P-III. doi: 10.1109/TELSKS.2003.1246173.
- [12] Entesari K, Saghati AP, Sekar V, Armendariz M. Tunable SIW structures: antennas, VCOs, and filters. IEEE Microw Mag. 2015;16(5):34–54. doi: 10.1109/MMM.2015.2408273.
- [13] Wu K. Integration and interconnect techniques of planar and nonplanar structures for microwave and millimeter-wave circuits – current status and future trend. 2001 Asia-Pacific Microw Conference. 2001. p. 411–6. doi: 10.1109/APMC.2001.985398.
- [14] Yan L, Hong W, Wu K, Cui TJ. Investigations on the propagation characteristics of the substrate integrated waveguide based on the method of lines. Microwaves, Antennas Propag, IEE Proc. 2005;152:35–42. doi: 10.1049/IP-MAP:20040726.
- [15] He F. Innovative microwave and millimetre-wave components and sub-systems based on substrate integration technology. Ph.D. thesis. Montreal, Canada: École Polytechnique de Montréal; 2011. https://publications.polymtl.ca/524/.
- [16] Che W, Deng K, Wang D, Chow Y. Analytical equivalence between substrate-integrated waveguide and rectangular waveguide. IET Microw Antennas Propag. 2008;2:35–41. doi: 10.1049/IET-MAP:20060283.
- [17] Campbell C, Traboulay I, Suthers M, Kneve H. Design of a stripline log-periodic dipole antenna. IEEE Trans Antennas Propag. 1977;25(5):718–21. doi: 10.1109/TAP.1977.1141653.
- [18] Carrel R. The design of log-periodic dipole antennas. 1958 IRE International Convention Record. 1966. p. 61–75. doi: 10.1109/ IRECON.1961.1151016.
- [19] Deslandes D, Wu K. Integrated microstrip and rectangular waveguide in planar form. IEEE Microw Wirel Compon Lett. 2001;11(2):68–70.
- [20] Aqlan B, Vettikalladi H, Alkanhal MA. Millimeter wave antenna with frequency selective surface (FSS) for 79 GHz automotive radar applications. Int J Microw Wirel Technol. 2016;9(2):281–90. doi: 10. 1017/S1759078716000027.
- [21] Jackson DR, Caloz C, Itoh T. Leaky-wave antennas. Proc IEEE. 2012;100(7):2194–206. doi: 10.1109/JPROC.2012.2187410.
- [22] Bai X, Qu SW, Ng KB, Chan CH. Sinusoidally modulated leaky wave antenna for millimeter – wave application. IEEE Trans Antennas Propag. 2016;64(3):849–55. doi: 10.1109/TAP.2015.2513089.
- [23] Jackson DR, Oliner AA, Balanis CA. Leaky-wave antennas. Modern antenna handbook. Hoboken, NJ, USA: Wiley; 2007. p. 325–67. doi: 10.1002/9780470294154.ch7.
- [24] Sarkar A, Lim S. 60 GHz compact larger beam scanning range PCB leaky-wave antenna using HMSIW for millimeter-wave applications. IEEE Trans Antennas Propag. 2020;68(8):5816–26. doi: 10. 1109/TAP.2020.2983.